Microporous and Mesoporous Materials 382 (2025) 113372

Contents lists available at ScienceDirect

Microporous and Mesoporous Materials

journal homepage: www.elsevier.com/locate/micromeso

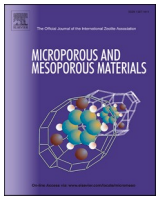

FTIR traced modification of defect-engineered UiO-66 for enhanced accessibility of zirconium sites

Vera V. Butova [a,b,*], Videlina R. Zdravkova [a], Olga A. Burachevskaia [b], Ivan E. Gorban [b], Mikhail A. Soldatov [b], Konstantin I. Hadjiivanov [a]

[a] Institute of General and Inorganic Chemistry, Bulgarian Academy of Sciences, Sofia, 1113, Bulgaria
[b] The Smart Materials Research Institute, Southern Federal University, Rostov-on-Don, 344090, Russia

ARTICLE INFO

Keywords:
Formic acid
Benzoic acid
Carbon monoxide
CD_3CN
XANES
MOF
Infrared spectroscopy

ABSTRACT

This research focuses on identifying the accessibility of active sites within the defect-engineered UiO-66 framework. The task is particularly challenging due to reversible changes in the framework during dehydroxylation: the loss of μ_3-OH groups with simultaneous reduction of the Zr coordination number and the possible creation of Zr^{4+} Lewis acid sites in defect MOFs. We used in-situ FTIR and XANES analyses, as well as interaction with probe molecules, to monitor the changes in Zr coordination and the host-guest interaction. The defects were introduced using benzoic acid as a modulator, which coordinated to Zr^{4+} in defective pores. Our results showed that the UiO-66 sample synthesized with benzoic acid contained defects, but these were concealed under benzoate residues and thus inaccessible. Standard washing and heating did not remove benzoate anions. Dehydroxylation of the sample leads to the development of "hidden" Lewis acidity: some Zr^{4+} sites were not able to form complexes with the weak base CO, but they interact with the stronger bases acetonitrile. Additionally, in-situ XANES analysis revealed that the effect of acetonitrile adsorption is similar to that of water rehydration. Treatment of the sample with HCl and DMF led to the replacement of benzoates with formate ions, exposing the bare Zr^{4+} sites within the defective pores. These cationic sites acted as true Lewis acids and were able to coordinate both CO and acetonitrile. Our findings emphasize that the active sites in UiO-66 highly depend on synthesis conditions and post-synthetic treatments. Comprehensive site-specific methods are crucial for accurately predicting and identifying these active sites.

1. Introduction

Zirconium-based metal-organic frameworks (MOFs) represent a class of porous materials known for their exceptional thermal and chemical stability. These MOFs consist of Zr-O clusters coordinated with carboxylic linkers, forming strong covalent bonds and achieving high coordination numbers of Zr^{4+}, contributing to their remarkable stability. UiO-66, a prominent family member, was first reported in 2008 [1]. It is composed of $Zr_6O_4(OH)_4$ clusters linked by 12 terephthalate linkers (BDC), resulting in a cubic structure containing both tetrahedral and octahedral pores [2,3]. UiO-66 has paved the way for a diverse family of isoreticular MOFs with various linkers, typically dicarboxylate acids featuring carboxylic groups in the para-position [2,4,5].

The UiO-66 comprises $Zr_6O_4(OH)_4$ clusters (Fig. 1b). However, treatment under vacuum at elevated temperatures, referred to as activation, leads to removing two water molecules and transforming the cluster to Zr_6O_6 (Fig. 1a). After activation, the cluster no longer contains μ_3-OH groups, and zirconium ions reduce their coordination numbers from 8 to 7 [6]. Notably, this process is reversible, and the samples can be rehydrated.

In the ideal structure of UiO-66, zirconium-oxygen clusters coordinate with 12 BDC linker molecules. This high connectivity renders these MOFs exceptionally tolerant to defects. A coordination modulation approach was proposed to intentionally introduce defects [7–11]. In this approach, a monocarboxylic acid serves as a modulator and is added to the reaction mixture alongside the linker, with a higher modulator concentration than the linker. The modulator and linker compete to bond with Zr^{4+} ions within the reaction mixture. The higher modulator concentration favors its interactions with the inorganic node. However, the modulators possess only one carboxylic group and cannot bridge two Zr_6O_6 clusters. Consequently, crystal growth occurs when linkers replace modulators. In some cases, Zr^{4+} ions within the MOF crystal

* Corresponding author. Institute of General and Inorganic Chemistry, Bulgarian Academy of Sciences, Sofia, 1113, Bulgaria.
E-mail address: v.butova@svr.igic.bas.bg (V.V. Butova).

https://doi.org/10.1016/j.micromeso.2024.113372
Received 5 August 2024; Received in revised form 11 October 2024; Accepted 14 October 2024
Available online 15 October 2024

retain modulators in their coordination sphere instead of linkers, forming defects. As a result, when a linker is missing, defect pores form, and vacancies appear on two opposite Zr_6O_6 clusters. The effect of modulators on MOF formation varies based on their concentration and properties. It has been reported that increasing the acid strength of the modulator promotes defect formation in MOFs [7,12,13]. Additionally, the size of the modulator molecule plays a role in this process. Benzoic acid, for example, has a molecular size similar to the BDC linker, which leads to the creation of a relatively high number of defects per node. However, at high concentrations of benzoic acid, it becomes difficult for BDC to replace it due to its larger size.

Temporary anions balance the excess positive charge of Zr^{4+} ions in these defect sites. When UiO-66 is synthesized in DMF, formate ions may be present, as DMF hydrolyzes in the presence of water at elevated temperatures, producing dimethylamine and formic acid. The formate group can bridge two Zr atoms at a vacancy site [14]. Studies have shown that formate ligands decompose at 473 K under high vacuum. However, other researchers have observed that alcohol treatment of activated UiO-66 forms alkoxides on the nodes [12,14]. Defect sites can be used for post-synthetic modifications when temporary residuals are replaced with desired species [15,16]. However, access to these sites may be blocked by residual modulators. For instance, bulky benzoic acid residues can completely obstruct zirconium sites, making them inaccessible to gas molecules or for post-synthetic modifications [17,18].

In summary, UiO-66 is a complex system containing various potential active sites, which can be altered during the activation procedure or blocked by modulator anions. Generally, the active sites within Zr-O clusters of UiO-66 can be considered in three categories. Firstly, $Zr_6O_4(OH)_4$ clusters initially contain μ_3-OH groups with weak Brønsted acidity [17,19]. The activation process removes these sites, reducing Zr's coordination number and allowing other molecules to replace the segregated μ_3-OH groups and form bonds with Zr^{4+}. Lastly, Zr^{4+} ions in defect pores, initially bonded with modulator molecules, become unsaturated and acquire Lewis acidic properties if these molecules are removed.

In this research, we assessed the accessibility of active sites in UiO-66 using FTIR analysis with probe molecules as the primary tool, complemented by XANES spectroscopy and other basic characterization methods. We compared two samples: the first was UiO-66 synthesized with benzoic acid as a modulator. This sample contained defective pores with benzoate ions bonded to zirconium sites. The second sample was obtained by treating the first sample with a DMF and HCl mixture to remove benzoate residues from the defective pores. Both samples were investigated in two states: hydrated and dehydrated. This comparison was used to evaluate and distinguish the effects of hydration-dehydration and compensating ions in defective pores on the composition and accessibility of active sites in the MOF.

2. Materials and methods

The starting materials zirconium tetrachloride ($ZrCl_4$), 1,4-benzene dicarboxylic acid (H_2BDC), N, N-dimethylformamide (DMF), benzoic acid (BA), hydrochloric acid (37 %) and methanol were purchased from Alfa Aesar and used without additional purification. Distilled water was purified via a Simplicity UV ultrapure water system.

2.1. UiO-66-BA

The samples were synthesized using the original procedure [15]. Briefly, $ZrCl_4$ was dissolved in DMF, and deionized water was added to the solution. BA was mixed in and stirred at room temperature until a clear solution was achieved. H_2BDC was added and dissolved. The molar ratio $ZrCl_4$: H_2BDC: H_2O: BA: DMF was 1: 1 : 3: 10 : 300. The reaction mixture was then placed in an oven and heated at 120 °C for 24 h. After synthesis, a white precipitate was collected by centrifugation and washed twice with pure DMF and methanol. Finally, the washed precipitate was dried at 60 °C overnight to obtain the UiO-66-BA sample.

2.2. UiO-66-FA

According to our previous research, using benzoic acid as a modulator produces defective pores, but its residues block Zr sites. To overcome this limitation, we applied a modification procedure based on [18] for the post-synthetic treatment of the UiO-66-BA sample. In this process, 50 mg of UiO-66-BA sample was combined with 15 mL of DMF and 0.625 mL of 8M HCl. The mixture was stirred thoroughly and loosely covered with a watch glass. Subsequently, the flask and its contents were heated at 100 °C for 24 h in a preheated oven. After the treatment, a microcrystalline powder formed, which was separated from the mixture via centrifugation. The powder was then washed three times with fresh

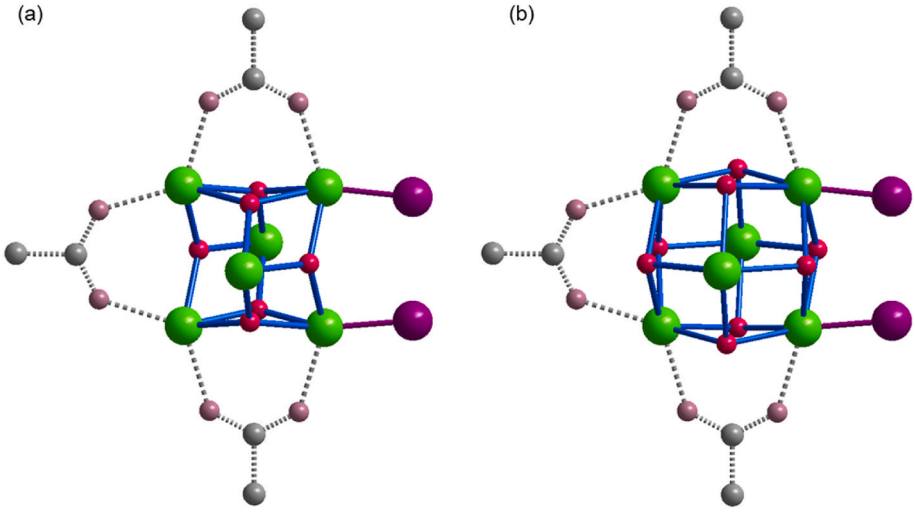

Fig. 1. Schematic representation of the zirconium-oxygen cluster of UiO-66. Part (a) represents the dehydrated Zr_6O_6 cluster, while part (b) represents the hydrated $Zr_6O_4(OH)_4$ cluster. Zirconium ions are depicted as green spheres, oxygen atoms in the clusters are shown as pink spheres, and bonds inside the clusters are highlighted with blue solid lines. Positions of linker molecules are depicted as carboxylic groups: gray spheres represent carbon atoms, dusty-pink spheres represent oxygen, and dashed gray lines represent bonds in carboxylic groups. Both clusters are presented with defective sites. One linker molecule is missing in each of them, and zirconium is coordinated with temporary compensating ions, shown as purple spheres. The crystal structure was elaborated according to crystallographic data from Ref. [11].

DMF. Lastly, the precipitate was separated from the solvent by centrifugation and dried overnight in an oven set to 60 °C. Following this treatment, the sample was referred to as UiO-66-FA in the text.

2.3. Characterization

X-ray powder diffraction (XRD) profiles were obtained using a D2 PHASER diffractometer (Bruker Corporation, Germany) in the 2θ range of 5–90° with a step size of 0.01 and CuKα radiation with a wavelength (λ) of 1.5417 Å. The profile analysis was conducted using Jana 2006 software [20].

For ATR-IR spectra measurements, an ex-situ analysis was performed on a Bruker Vertex 70 spectrometer, covering a range from 5000 to 500 cm^{-1} with a resolution of 1 cm^{-1}. The data was accumulated through 64 scans using an MCT detector and a Bruker Platinum ATR attachment.

N_2 sorption isotherms were recorded at −196 °C applying ASAP2020. Prior to the measurements, samples were degassed for 10 h at 150 °C in a dynamic vacuum. Specific surface areas (SSA) were calculated according to the BET model. Pore size distribution was calculated using the adsorption branch of the respective isotherm according to the Horvath-Kawazoe model for cylindrical pores.

In situ FTIR spectra of the self-supporting pellets were recorded using a Nicolet 6700 FTIR spectrometer. For these measurements, 64 scans were accumulated at a spectral resolution of 2 cm^{-1}. The self-supporting pellets were prepared from the sample powders and analyzed directly in a specially designed IR cell, enabling measurements at both ambient and low (approximately −173 °C) temperatures. The IR cell was connected to a vacuum adsorption apparatus with a residual pressure below 10^{-3} Pa. Before the adsorption experiments, the samples were activated by evacuation at different temperatures. The adsorption experiments were conducted by introducing either 5 mbar of CO (Merck, purity 99.5 %) or CD_3CN (Merck, deuteration degree 99.96 %) directly into the IR cell. Afterward, the adsorbed gases were diluted, and the cell was evacuated for different durations as part of the experimental procedure.

The NMR spectra were recorded on a Bruker AVANCE NEO 600 MHz spectrometer equipped with a 5 mm Prodigy probehead at a proton operating frequency of 600.18 MHz. The spectra were measured without spinning the sample at a temperature of 298 K. The NMR spectra for quantitative analysis were measured with a pulse sequence with water suppression *zgesgppe* using the following experimental parameters, optimized for quantitative measurements: 90° hard excitation pulse, spectral width 10.96 ppm, 64 K time domain data points, 16 scans, 10s water suppression time and a relaxation delay of 50 s to ensure complete relaxation for all signals. The spectra were Fourier transformed after zero filling to 128 K, giving a digital resolution in the frequency domain of 0.10 Hz/pt. Careful manual phase and baseline corrections were made prior to signal integration. Before conducting measurements, UiO-66 samples were dissolved in a deuterated alkaline medium (1 M NaOD in D_2O) following the method described by Shearer et al. [13]. The powder was added to the alkaline solution, thoroughly mixed, and left for 24 h. Afterward, the suspension was centrifuged, separating the solid and liquid components. All organic compounds were transferred into the liquid phase as their corresponding sodium salts and used for NMR analysis. The white precipitate contained hydrated ZrO_2.

The Zr K-edge XANES spectra were measured at the Structural Materials Science end-station [21] at the Kurchatov Synchrotron Radiation Source (Moscow, Russia). The Si(220) channel-cut crystal monochromator was selected to obtain $\Delta E/E = 2{\cdot}10^{-4}$ energy resolution. Signals were detected using ionization chambers. Pellets of the samples mixed with cellulose as an agent for binding and dilution have been prepared to give transmission signals above the Zr absorption edge of μd of about 1. The samples were transferred to a custom in situ cell equipped with a gas line and a heater. Data were averaged over three scans, measured at the same position of a pellet for each sample. The standard data reduction was performed using the Demetra package [22]. The energy was calibrated to the first infection point of a metal Zr spectrum to 18.998 keV (the first maximum of the first derivative). Data were pre- and post-edge background corrected with a linear and a polynomial function, respectively, and were normalized to an edge jump of one to enable comparison of spectra using the Athena program of the Demetra software package. The experiment was performed as follows: i) The measuring cell was evacuated to a pressure of 5.5×10^{-5} bar and heated to 250 °C to activate the UiO-66 structure. ii) The cell was then cooled to room temperature, and water vapor was introduced to ensure complete cleaning of the solvents. iii) The cell was evacuated again to a pressure of 5.5×10^{-5} bar. iv) Acetonitrile vapor was introduced into the cell to occupy the free positions of the active zirconium centers. v) The cell was once again evacuated and heated to 250 °C to create active centers and remove acetonitrile. vi) Finally, the sample was cooled to room temperature at a pressure of 5.5×10^{-5} bar, and acetonitrile was reintroduced into the cell.

Raman scattering experiments were conducted using an inVia Raman microscope. Measurements utilized the 532 nm (green) diode laser. Spectral analysis was carried out using the Origin 9 software. Spectra were collected in the 550–1700 cm^{-1} range.

3. Results

3.1. Crystal structure and thermal analysis

Fig. 2a displays the XRD patterns of UiO-66-BA and UiO-66-FA samples. Both samples showed a single-phase UiO-66-type structure. All reflections were identified in a cubic symmetry, with the space group Fm-3m. Despite the post-synthetic treatment, there was no structure collapse or formation of any new phases (Table S1, Fig. S1 in SI). The UiO-66-BA sample exhibited a slightly larger lattice constant compared to the UiO-66-FA sample (Table 1). This effect is believed to be linked to the removal of guest molecules and modulator residuals from the pores during the treatment.

Fig. 2b demonstrates the TGA and DSC curves of UiO-66-BA and UiO-66-FA samples. Both of them contained three steps of weight loss. The first step occurs in the temperature range of 50–150 °C. It corresponds to the removal of physically adsorbed water molecules. The next step in the temperature range of 150–350 °C refers to the elimination of DMF and other bonded guest molecules. A slight inflection at a temperature of about 250 °C is associated with the dehydroxylation of the samples and transformation of the $Zr_6O_4(OH)_4$ cluster to the form of Zr_6O_6. The theoretical weight loss of ideal UiO-66 is 55.6 % and 54.6 % according to the formula unit $Zr_6O_4(OH)_4(BDC)_6$ and $Zr_6O_6(BDC)_6$, respectively (see calculation details in SI, Part 2). The UiO-66-BA sample demonstrated a weight loss of 55.8 %, which is very close to the theoretical value. The UiO-66-FA sample exhibited lower weight loss, estimated at 42.9 %. It could indicate that a more bulky BA modulator was replaced with a less bulky one. These results are in good agreement with a previous report [18].

3.2. Porosity

Low-temperature N_2 sorption isotherms are shown in Fig. 3a. Both isotherms correspond to type I according to the IUPAC notification. These shapes of isotherms are typical of microporous materials. In the P/P_0 range of 0.8–1.0, we noticed hysteresis loops indicating capillary condensation of N_2 in spaces between monodisperse nanoparticles. Specific surface areas were calculated according to the BET model and were estimated as 1335 $m^2\ g^{-1}$ for the UiO-66-BA sample and 1715 $m^2\ g^{-1}$ for the UiO-66-FA sample (For detailed information, refer to the SI, part 3). So, modification of the UiO-66-BA sample resulted in an increase of its specific surface area by 1.3 times. Fig. 3b represents pore size distribution for pristine and modified UiO-66 samples. The first two picks at 8 and 10 Å correspond to regular pores in the UiO-66 framework. Both samples contained such pores. However, the UiO-66-FA sample showed an additional pick at about 20–25 Å, indicating

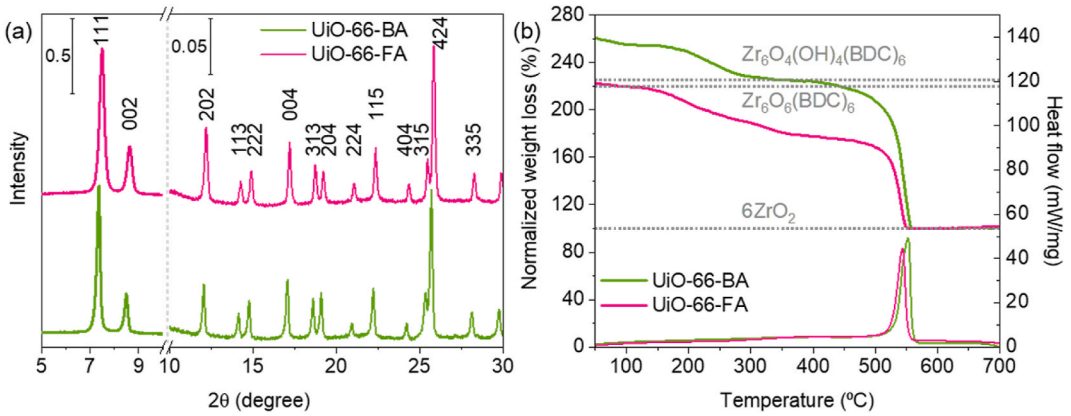

Fig. 2. (a) XRD patterns of the UiO-66-BA and UiO-66-FA samples. Profiles were shifted along the intensity axis. Intensities were multiplied by ten for 2θ-region after dotted lines for better representation. Numbers designate Miller indices. (b) TGA and DSC curves of UiO-66-BA and UiO-66-FA samples. The TGA curves were normalized based on the assumption that each mole of the UiO-66 formula unit converts to 6 mol of ZrO_2 during the calcination process. Additionally, 6 mol of ZrO_2 was considered to be 100 %. For detailed information, refer to the SI. Gray dashed lines show the theoretical positions of the plateau according to formula unit $Zr_6O_4(OH)_4(BDC)_6$ and $Zr_6O_6(BDC)_6$.

Table 1
Some characteristics of UiO-66-BA and UiO-66-FA samples. SSA stands for specific surface area. Pore volume was measured at $P/P_0 = 0.97$.

Sample	Structure		N_2 sorption	
	a, Å	V, Å^3	SSA, m^2·g^{-1}	Pore volume, cm^3·g^{-1}
UiO-66-BA	20.7731 (4)	8964.1 (3)	1345	0.646
UiO-66-FA	20.7610 (5)	8948.4 (4)	1812	0.796

accessible defect pores.

3.3. IR and Raman

Fig. 4 presents the IR and Raman spectra of UiO-66-BA and UiO-66-FA samples. Treatment with HCl and DMF did not cause any significant changes in the fingerprint region of the spectra, suggesting no alterations in the UiO-66 structure (Fig. S4). However, certain bands at 937, 1025, 1068, 1139, and 1177 cm^{-1} vanished after treatment. These bands correspond to vibrations of benzoate ions [7,17,23] (see detailed description in Table S2). The spectrum of the UiO-66-FA sample did not contain these benzoate modulator peaks, indicating the removal of the benzoate modulator. A weak band at 1060 cm^{-1} in the spectrum of the UiO-66-FA sample can be attributed to the out-of-plane vibrations of C-H bonds in formate ions, which have replaced benzoate ions [24,25]. These findings are also supported by the Raman spectra (Fig. 4b). The bands at 618 and 1005 cm^{-1} in the spectrum of the UiO-66-BA sample were assigned to benzoate residuals [26]. These bands were not observed in the spectrum of the UiO-66-FA sample. A shoulder at 1070 cm^{-1} in the Raman spectrum of UiO-66-FA could be due to the δ_{as} (CH) vibrations of formate ions [26].

3.4. In situ FTIR

3.4.1. Activation

We traced the activation procedure for UiO-66-BA and UiO-66-FA samples using *in-situ* FTIR spectroscopy. After synthesis, each sample was evacuated at the respective temperature, cooled down under a dynamic vacuum, and placed into an IR beam without exposure to air. Treating the samples in a dynamic vacuum at room temperature removed physically adsorbed water molecules from the pores, revealing a region in the IR spectra from 2600 to 3800 cm^{-1}. Fig. 5 shows selected areas for each sample evacuated at room temperature, at 250 °C, and after subsequent rehydration. The rehydration process included two steps: exposure to 5 mbar of water vapor at room temperature, followed by evacuation at room temperature and holding under dynamic vacuum for 15 min. The spectra of both UiO-66-BA and UiO-66-FA samples contained a band at 3674 cm^{-1}, attributed to the stretching O-H modes of μ_3-OH groups [17,19,26]. Evacuation at 150 °C increased the peak intensity because of destruction of some OH···OH_2 and OH ··· DMF adducts.

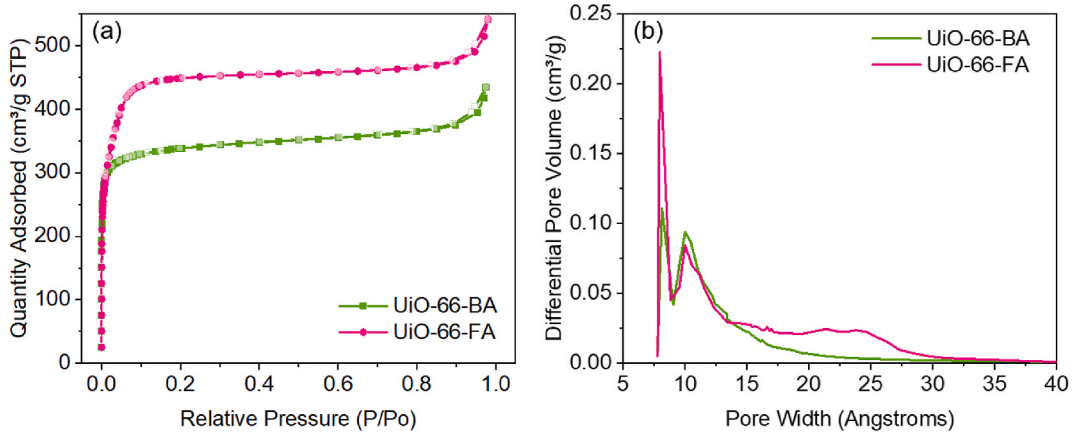

Fig. 3. (a) N_2 sorption isotherms of UiO-66-BA (green square markers) and UiO-66-FA (pink circle markers) samples. Filled markers represent adsorption branches of isotherms; empty markers show description ones. (b) Pore size distribution for UiO-66-BA (green plot) and UiO-66-FA (pink plot).

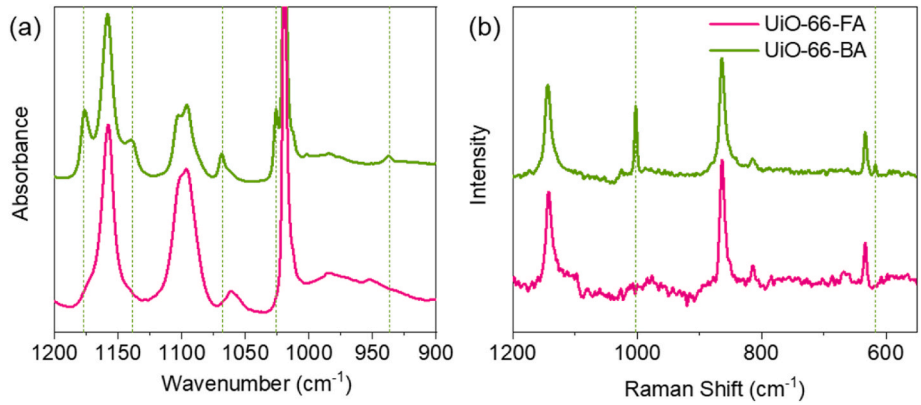

Fig. 4. IR spectra (a) and Raman spectra (b) of samples UiO-66-BA and UiO-66-FA. Dashed lines highlight bands assigned to benzoate ions.

Further increasing the evacuation temperature led to a reduction in peak intensity due to the dehydroxylation process. Consequently, activation at 250 °C resulted in the transformation of the $Zr_6O_4(OH)_4$ cluster to Zr_6O_6 in both samples (Fig. S6). Rehydration of the samples led to the restoration of the corresponding peak intensity, indicating the reversibility of the dehydration process (Fig. S7a).

It is also noteworthy that after the first rehydration, the position of the μ_3-OH peak was slightly shifted, while subsequent dehydroxylation-rehydroxylation procedures did not affect the peak position (Fig. S7a). It has been reported that the position of the μ_3-OH peak is strongly influenced by the functional groups of linkers and the compensating anions at defective Zr sites, such as benzoate residues [12]. We infer that this shift is connected to the evacuation of DMF guest molecules from the pores of the MOF. This is confirmed by the fact that some peaks (highlighted with arrows in Fig. 4) disappeared after the first activation and did not reappear during the rehydration process. These peaks were assigned to DMF vibrations (see Table S2).

After the first evacuation at room temperature, we observed peaks in the 3030–3080 cm^{-1} region in the spectrum of the UiO-66-BA sample (Fig. 5a). These peaks are assigned to benzoate vibrations (Table S2). Subsequent activation and rehydration procedures did not lead to the loss of these peaks, suggesting that benzoate residues cannot be removed through heating and evacuation. The spectrum of the UiO-66-FA sample after room temperature evacuation did not contain these bands, indicating that the modification procedure successfully removed benzoate residues. The new bands in the 2850–2955 cm^{-1} region of the spectrum of the UiO-66-FA sample were attributed to formate ions, which replaced the benzoate ions [18,27]. The removal of terminal ions in Zr-MOFs has been reported to trigger the formation of reactive OH/H_2O pairs, with characteristic bands located around 3720–3780 cm^{-1}, as observed in NU-1000 [28,29]. However, when the UiO-66-FA sample was activated at 250 °C, no such bands appeared in the spectra. This does not definitively prove that no formate ions were removed during the evacuation at 250 °C; in fact, we suggest that some were. Nevertheless, the sites were not terminated by the reactive OH/H_2O groups reported in other cases [28,29].

We used NMR spectroscopy to study the obtained samples. First, the samples were dissolved in NaOD in D_2O, and the solid product was separated, leaving a solution of organic components for NMR analysis [13]. The spectra were normalized, with the BDC peak set at 100 %. The NMR spectrum associated with the UiO-66-BA sample shows peaks in the 7.4–8 ppm region, indicating the presence of benzoate ions (Fig. 6). The BDC-to-BA ratio was estimated as 1:0.35. Notably, even after activation at 250 °C, the UiO-66-BA sample still contained benzoate ions, which is consistent with FTIR data. In contrast, the UiO-66-FA sample contained only trace amounts of benzoate ions, as indicated by the very weak NMR peaks. This confirms that treatment with HCl successfully removed benzoate ions from the UiO-66 structure.

Additionally, intense peaks at around 2.3 ppm and 8.5 ppm were observed in the spectra of UiO-66-BA and UiO-66-FA samples activated at RT (Fig. 6a). These peaks correspond to dimethylamine (2.3 ppm) and formate ions (8.5 ppm), indicating that DMF decomposition occurred during sample preparation in the alkaline medium [13]. The presence of these peaks suggests that successive heating at 60 °C, followed by room temperature evacuation, did not completely remove DMF from the UiO-66 pores. This observation is consistent with the FTIR results.

Comparing the samples activated at 250 °C, the UiO-66-BA sample contained only trace amounts of formate ions, while the UiO-66-FA sample showed a significant peak at 8.5 ppm (Fig. 6b). This suggests that formate ions, formed during HCl treatment, replaced benzoate

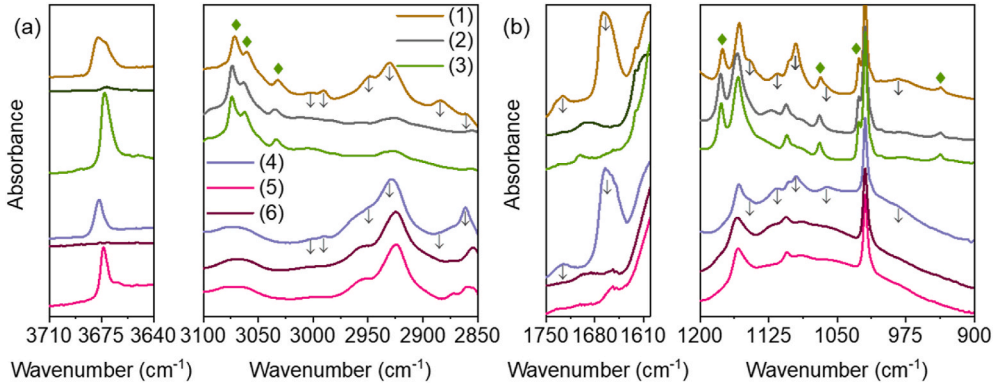

Fig. 5. Selected regions of IR spectra were measured for (1) UiO-66-BA evac at RT, (2) UiO-66-BA evac at 250 C, (3) UiO-66-BA rehydrated and evacuated at RT; (4) UiO-66-FA evac at RT, (5) UiO-66-FA evac at 250 C, (6) UiO-66-FA rehydrated and evacuated at RT. Green diamonds highlight bands attributed to BA vibrations. Dashed arrows highlight bands corresponding to DMF vibrations.

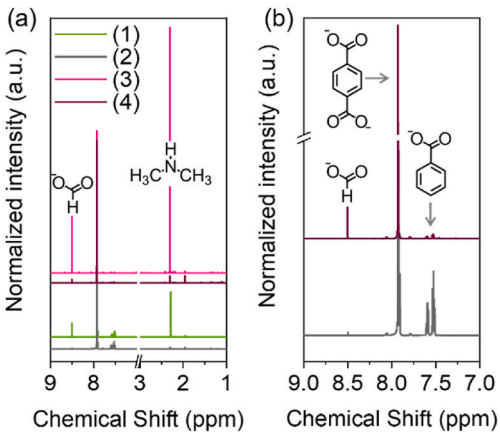

Fig. 6. (a) Dissolution/^{1}H NMR spectra obtained on the UiO-66-BA sample evacuated at RT (1) or at 250 °C (2), UiO-66-FA sample evacuated at RT (3) or at 250 °C (4). Part (b) shows the aromatic region from 7.0 to 9.0 ppm of the UiO-66-BA (2) and UiO-66-FA (4) samples evacuated at 250 °C.

residues in the defect pores. However, the amount of formate ions was about 20 times lower than that of the benzoate ions, possibly due to the removal of formate during activation at 250 °C.

It has been reported that the thermal stability of UiO-66-type MOFs strongly correlates with defect concentration [8,30]. Additionally, given our observation of the reversibility of the hydration-dehydration process in the FTIR spectra, we decided to check the stability of the structure using XRD. We slowly heated the UiO-66-BA and UiO-66-FA samples in a dynamic vacuum and activated them at 250 °C for 15 min, replicating the FTIR experiment. After cooling down and refilling the activation vessel with N_2, the samples were exposed to air and rehydrated. Fig. 7a shows the XRD profiles of the UiO-66-BA sample before and after activation (for UiO-66-FA, see SI Fig. S7b). This treatment did not alter the crystal structure of the sample. We observed a slight decrease in lattice constants, which we attribute to the evacuation of guest molecules from the pores. The same trend was observed for the UiO-66-FA sample. Thus, we concluded that the activation of synthesized samples did not lead to structural collapse. However, it should be noted that treating these samples in a dynamic vacuum at 250 °C for 6 h or at 275 °C for half an hour resulted in amorphization.

Next, we examined the local coordination of Zr^{4+} via X-ray absorption spectroscopy. Fig. 7b compares the XANES spectra for as-synthesized, activated, and rehydrated UiO-66-BA. It is evident that the main peak position shifts to higher energies after activation. The second spectral feature at 18,080 eV also shifts to higher energy. The intensities of these peaks visibly decrease. Rehydroxylation leads to an inverse effect: the intensities of the main and second peaks slightly increase, and peak positions shift to lower energies, although they do not return to their initial values. Our results for the intact and activated samples show a trend similar to previous studies on UiO-66 activation [6]. However, we did not observe complete reversibility of dehydration in the XANES spectra. In the present study, the XANES spectral shape does not fully return to its initial state, as seen in the as-synthesized sample. This trend was also observed in the FTIR spectra, where rehydration after the first activation did not result in the complete restoration of the spectral shape and peak positions. We observed shifts in some UiO-66 bands and the disappearance of bands attributed to DMF.

Summarizing all the experimental data from FTIR and XANES spectroscopy and XRD analysis, we conclude that after synthesis, UiO-66 contains DMF molecules inside the pores, which affect the framework behavior (increasing lattice constants, changing vibrations of functional groups, and altering Zr^{4+} coordination). Activation at 250 °C results in the evacuation of guest molecules, changing the coordination of Zr^{4+} in the UiO-66 framework. Rehydration results in the adsorption of water molecules, and this process is completely reversible. While short evacuation at 250 °C does not cause structural collapse according to XRD, prolonged treatment can lead to amorphization. We suggest that this correlates with defect concentration, highlighting that the activation procedure is crucial but must be carried out with caution.

3.4.2. CO adsorption

Carbon monoxide (CO) is the most commonly used probe molecule for identifying acidic sites in solids, especially in MOFs [17,26,31,32]. We conducted experiments involving low-temperature adsorption of CO on the UiO-66-BA and UiO-66-FA samples evacuated at room temperature (RT) or at 250 °C. This allowed us to compare the active sites in both hydroxylated and dehydroxylated samples.

Fig. 8a represents the spectra of CO adsorbed on UiO-66-BA and UiO-66-FA samples evacuated at RT (see also Fig. S8 in SI). Note that evacuation at RT does not lead to dehydroxylation, and the $Zr_6O_4(OH)_4$ cluster contains μ_3-OH groups with Brønsted acidic properties that can form an H-bond with CO. A strong band at 2152 cm^{-1} dominates in the carbonyl region. This band is assigned to the stretching vibration of the CO molecule H-bonded to the μ_3-OH group via the carbon atom: μ_3-OH···C ≡ O [17,19,26]. In addition, weak bands at 2131, 2136, and 2124 cm^{-1} were observed. The bands at 2131 and 2136 cm^{-1} arise from physically adsorbed CO [17,33]. The weak band at 2124 cm^{-1} was attributed to the CO bonded to the μ_3-OH group via its oxygen atom: μ_3-OH ····O ≡ C [19,33,34]. The intensity of this band is much lower than for the μ_3-OH···C ≡ O adducts, indicating the preferred H-bonding of carbon monoxide through its carbon atom. Adsorption of CO was also accompanied by a shift in the position of the band attributed to vibrations of the μ_3-OH group (Fig. 8b) due to the formation of the μ_3-OH···C ≡ O adducts. In summary, after evacuation at RT, both samples contained only one type of active site for CO adsorption - μ_3-OH groups.

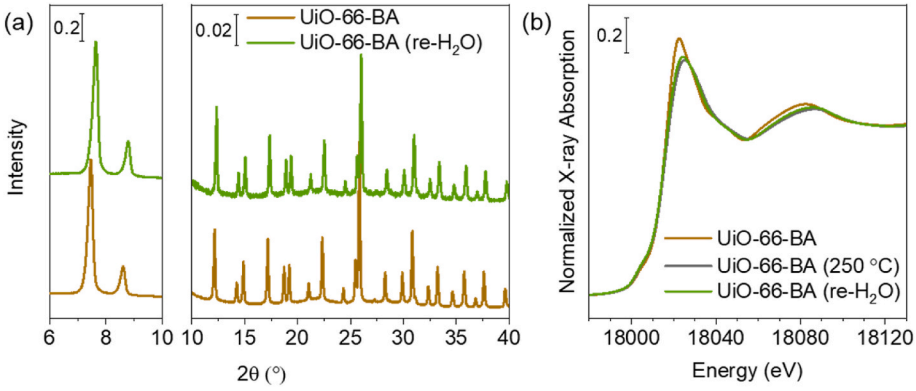

Fig. 7. (a) XRD patterns of as-synthesized UiO-66-BA sample (beige) and the same sample after activation at 250 °C and rehydration (green). (b) In situ X-ray absorption spectra were collected as synthesized (beige), activated (gray), and hydrated (green) UiO-66-BA.

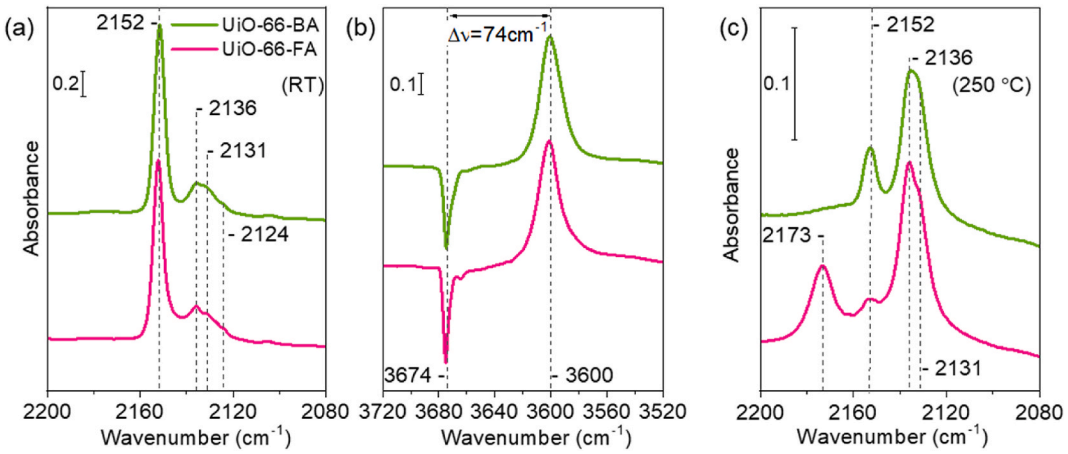

Fig. 8. FTIR spectra registered after low-temperature adsorption of CO (1 mbar equilibrium pressure) on UiO-66-BA and UiO-66-FA samples evacuated at room temperature (a, b) and at 250 °C (c). Part (b) illustrates the difference between the spectrum of the corresponding sample evacuated at room temperature before and after exposure to CO gas at a pressure of 1 mbar at liquid nitrogen temperature.

Evacuation of the samples at 250 °C led to a strong decrease in intensity of the bands around 3674 cm^{-1} characterizing μ_3-OH groups. Hence, the pretreatment resulted in almost full conversion of the $Zr_6O_4(OH)_4$ cluster to Zr_6O_6. (Fig. S6). Fig. 8c illustrates the spectra of CO adsorbed on UiO-66-BA and UiO-66-FA samples evacuated at 250 °C. In this case, the most intense bands were those of physically adsorbed CO (2131 and 2136 cm^{-1}). Low-intensity bands at 2152 cm^{-1} were observed in the spectra of both samples and were attributed to CO adsorbed on residuals of μ_3-OH groups. Notably, the UiO-66-BA sample contained a higher amount of these groups, as indicated by the higher intensity of the band at 2152 cm^{-1}. In contrast, the UiO-66-FA sample contained only small residuals of μ_3-OH groups. Consequently, the shift in the position of the band at 3674 cm^{-1}, attributed to vibrations of the μ_3-OH group due to the formation of μ_3-OH···C ≡ O adducts, was traceable only in the UiO-66-BA sample (Fig. S9 c). No pronounced peaks were observed in the 3500-3700 cm^{-1} region in the spectra of the UiO-66-FA sample, likely because they were at the noise level (Fig. S9 d). Thus, the dehydration process was facilitated by removing benzoate residuals from defective pores. It has been reported that larger pores restrain small molecules more weakly, resulting in easier evacuation of physisorbed water [7]. We hypothesize that the removal of benzoate residuals enlarged the defect pores and decreased transport restraints, leading to faster dehydration.

The spectrum of CO adsorbed on the UiO-66-FA sample revealed a new band at 2173 cm^{-1}, while the spectrum of the UiO-66-BA sample did not exhibit such a band. The 2173 cm^{-1} band was attributed to vibrations of CO molecules bonded to coordinatively unsaturated Zr^{4+} sites originating from defective pores and formed after removal of the formate ions [17,33]. The absence of such bands in the spectrum of the UiO-66-BA sample indicates that these zirconium sites are blocked by the benzoate modulator and are not able to interact with CO molecules. In contrast, the presence of this band in the UiO-66-FA sample activated at 250 °C demonstrates that post-synthetic modification resulted in the removal of benzoate ions, revealing zirconium sites in defect pores for further interactions (Table 2).

In conclusion, we can infer that the activated UiO-66-FA sample contained accessible Zr^{4+} sites, while in the UiO-66-BA sample, zirconium ions in defective pores are saturated with the BA modulator.

3.4.3. CD_3CN adsorption

Acetonitrile serves as a prevalent probe molecule in FTIR spectroscopy due to its distinctive properties. Possessing base properties, acetonitrile readily interacts with acidic sites, making it an ideal candidate for investigating surface properties. In comparison to carbon monoxide, acetonitrile exhibits a more pronounced basic character. In our experiments, we opted for using deuterated acetonitrile (CD_3CN) instead of regular acetonitrile (CH_3CN) because of the absence of split of the C-N modes due to Fermi-resonance [26].

Table 2
Positions of bands assigned to respective active sites, with values provided in cm^{-1}. ND indicates when a band was not detected. (vw) denotes a very weak band, and (w) designates a weak band.

Active site	μ_3-OH		Zr^{4+} in regular pores		Zr^{4+} in defect pore	
Probe molecule	CO	CD_3CN	CO	CD_3CN	CO	CD_3CN
Sample						
UiO-66-BA (RT)	2152	2277	ND	ND	ND	ND
UiO-66-FA (RT)	2152	2277	ND	ND	ND	2303
UiO-66-BA (250 °C)	2152 (w)	2277 (w)	ND	2300	ND	ND
UiO-66-FA (250 °C)	2152 (vw)	2277 (vw)	ND	2300	2173	2303

Fig. 9a depicts the spectra of CD_3CN adsorbed on samples activated at room temperature. In both spectra, prominent bands at 2262 and 2277 cm^{-1} are observed. These bands are attributed to the C-N stretching modes of physically adsorbed acetonitrile (2262 cm^{-1}), and CD_3CN adsorbed on μ_3-OH-groups of $Zr_6O_4(OH)_4$ clusters (2277 cm^{-1}) (Table 2). The interaction between μ_3-OH-groups and CD_3CN is also evident from the redshift in the positions of μ_3-OH-group bands by 228 cm^{-1} induced by the exposure to CD_3CN (Fig. 9b). This shift, greater than that observed for CO adsorption, underscores the stronger basic properties of acetonitrile.

Additionally, a band at 2303 cm^{-1} emerges in the spectrum of UiO-66-FA (Fig. 9a), indicating the interaction of CD_3CN with Zr^{4+} ions. The same band is practically absent from the spectrum of UiO-66-BA. Therefore, we infer that these adsorption sites are bare Zr^{4+} ions in defect pores formed as a result of the removal of modulator anion. Normally, such sites should be blocked by adsorbed water. However, acetonitrile has a relatively high proton affinity (779.2 kJ mol^{-1}), higher than that of H_2O (691 kJ mol^{-1}) [19,35], and can replace pre-adsorbed water.

Upon activation at 250 °C, the dehydration process and loss of μ_3-OH-groups occur, leading to only faint peaks at 2277 cm^{-1} (Fig. 9c). Notably, bands in the 2300-2305 cm^{-1} region become visible in the spectra of both samples. It is important to highlight that the peak position for UiO-66-FA has slightly shifted, becoming broader and more intense compared to UiO-66-BA. Therefore, it seems that the acetonitrile peak at ca. 2300 cm^{-1} on the UiO-66-FA sample is a composite and

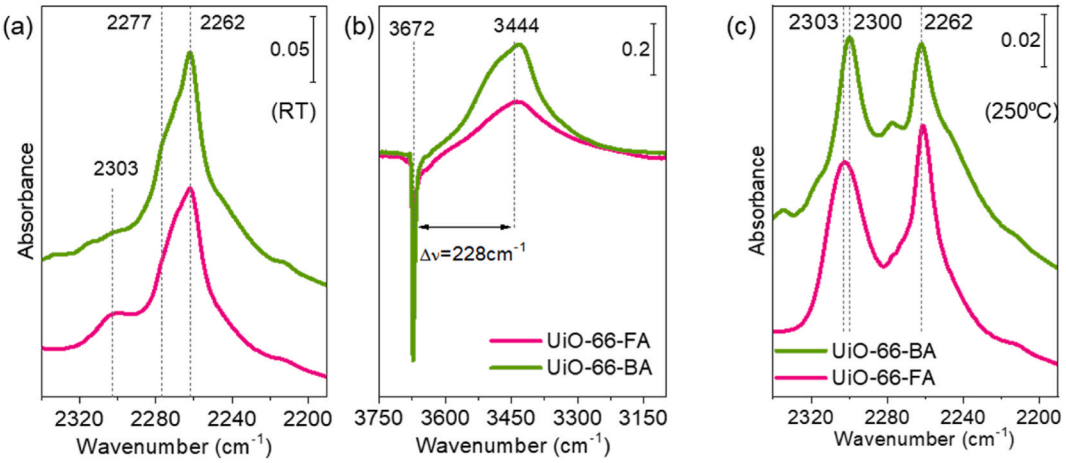

Fig. 9. FTIR spectra registered after adsorption of CD_3CN (3 mbar equilibrium pressure) on UiO-66-BA and UiO-66-FA samples evacuated at room temperature (a, b) and at 250 °C (c). Part (b) illustrates the difference between the spectrum of the corresponding sample evacuated at room temperature before and after exposure to CD_3CN vapor at a pressure of 3 mbar.

consists of two components (Fig. S12). The higher-frequency component corresponds to adsorption on bare Zr^{4+} sites in the defect pores and is at least partly detected with the sample evacuated at room temperature. These sites also are able to form carbonyl complexes (see Table 2). In addition, "hidden" Zr^{4+} sites are detected with both samples at 2300 cm^{-1}. These sites are located in the regular pores and are not able to interact with the weak base CO. However, they form complexes with CD_3CN. Note that a similar situation was previously found with a non-defect UiO-66 sample [19].

The interaction of acetonitrile with Zr^{4+} ions in regular pores is a rather interesting phenomenon. We measured the XANES spectra of Zr to investigate this interaction, using XANES as an element-selective method. Fig. 10 shows the pairwise comparison of spectra measured at different stages of the experiment.

The first pair shows almost no changes in spectral features after the hydroxylated sample was purged with acetonitrile vapor (Fig. 10a). The second pair clearly depicts shifts in peak intensity and energy position after the activated sample was purged with water vapor (Fig. 10b). The third pair shows changes in the spectral features after the activated sample was purged with acetonitrile (Fig. 10c). It is noteworthy that the changes in the spectra of activated UiO-66-BA after acetonitrile adsorption are similar to those observed after water adsorption. We propose that this indicates acetonitrile molecules change Zr^{4+} coordination in a similar way as water molecules do during the rehydration process, although these changes are less pronounced. Thus, we hypothesize that acetonitrile molecules are adsorbed at the positions of μ_3-OH groups, which become vacant after the dehydration process.

4. Discussion

Based on the results described above, we propose the following process description. In the first step, we synthesized UiO-66 using benzoic acid as a modulator, resulting in a MOF with defects where zirconium ions in defective pores were coordinated to benzoate anions. These anions are strongly bonded to zirconium and cannot be removed by heating in a dynamic vacuum, thus blocking the zirconium sites in the defect pores and making them coordinatively saturated and inaccessible.

However, the UiO-66-BA sample contains some active sites. Before dehydration, it can provide μ_3-OH-groups, which coordinate CO and CD_3CN probe molecules. After dehydration and the consequent removal of μ_3-OH-groups, CO molecules can only be physisorbed. In contrast, CD_3CN, being a strong base, can interact with Zr sites of the dehydrated UiO-66-BA sample. Given that the Zr-sites in the defective pores of the UiO-66-BA sample are blocked, we conclude that CD_3CN molecules are adsorbed on Zr-sites in the regular pores, which reduced their coordination number from 8 to 7 after dehydration.

Treating the UiO-66-BA sample with HCl and DMF removed the benzoate residues, resulting in the UiO-66-FA sample. This sample

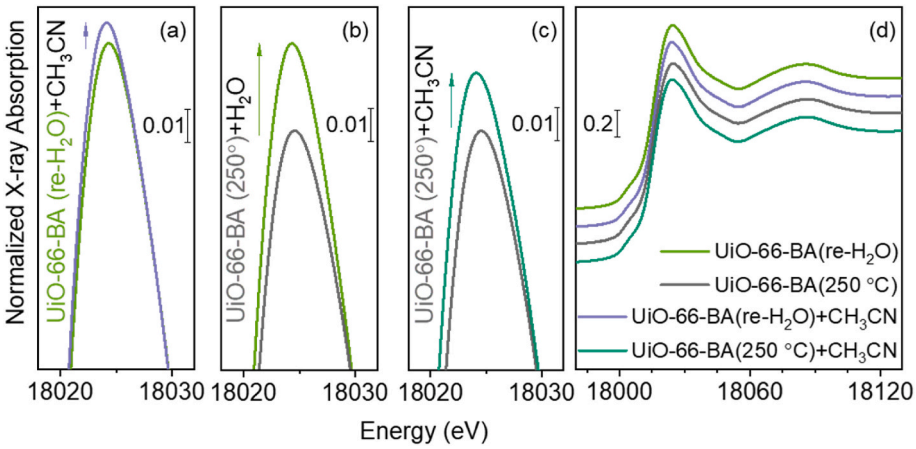

Fig. 10. In situ X-ray absorption spectra collected for rehydrated UiO-66-BA sample before and after CH_3CN adsorption (a); UiO-66-BA sample before and after evacuation at 250 °C (b); activated at 250 °C UiO-66-BA sample before and after CH_3CN adsorption (c); in situ X-ray absorption spectra collected at different stages of the experiment (d).

contained formate ions formed through the hydrolysis of DMF in an acidic medium, as shown in the reaction scheme (Fig. 11a) [36]. Formate ions are much less bulky than benzoate ions, increasing accessibility to defective pores. Moreover, during the activation procedure, these residues could be partially decomposed, producing additional bare Zr^{4+} sites that slightly differ in acidity from the other Zr-sites and can coordinate even weak bases as CO. Thus, this modification opened the Zr-sites in the defective pores.

This results in some alterations in the interaction with probe molecules. Before dehydration, CO was adsorbed only on μ_3-OH-groups, similar to the UiO-66-BA sample. However, after dehydration, the Zr-sites in the defect pores of the UiO-66-FA sample were able to adsorb CO probe molecules. A similar trend was previously observed for UiO-66, which was synthesized using HCl as a modulator [32]. In this case, the Zr sites in the defective pores became accessible only after thermal treatment.

When a strong base, such as CD_3CN, was used, we observed that some Zr sites in the defective pores of the UiO-66-FA sample were accessible even in a rehydrated state. For the dehydrated UiO-66-FA sample, we observed adsorption of acetonitrile on Zr sites similar to the UiO-66-BA case. The slightly broadened and shifted band allowed us to conclude that two types of Zr^{4+} sites can interact with CD_3CN in the dehydrated UiO-66-FA sample: Zr in defect pores and "hidden" Zr in regular pores.

5. Conclusions

In this research, we focused on identifying and assessing the accessibility of active sites within the UiO-66 framework. This is particularly challenging because the UiO-66 framework can undergo reversible changes during dehydration, leading to the reversible disappearance of μ_3-OH groups with Brønsted acidic properties and a reduction in the Zr coordination number from 8 to 7. Additionally, UiO-66 can contain defective pores where Z^{4+} ions, considered active sites with Lewis acidic properties, have accessibility that is highly dependent on synthesis conditions and post-synthetic treatment.

To introduce defects into the structure, we used benzoic acid as a modulator. Benzoic acid is a preferred modulator because it is solid at room temperature, non-corrosive, and does not cause DMF decomposition. Moreover, it forms strong bonds with Zr^{4+}, resulting in a high defect concentration in the material. However, these strong bonds also block Zr in defective pores. We used *in-situ* FTIR analysis with CO and acetonitrile probe molecules to trace the accessibility of Zr^{4+} ions. After synthesis, benzoate anions are coordinated to Zr^{4+} ions, thus blocking them for adsorption. Standard washing and heating procedures did not remove these benzoate residues from the defective pores of UiO-66. Although the samples with benzoate ions in defective pores could be dehydrated with the loss of μ_3-OH groups, they retained the benzoate ions.

We observed that the dehydrated sample with benzoate residues was still capable of adsorbing acetonitrile molecules. Since the Zr^{4+} ions in defective pores were blocked, we inferred that the acetonitrile was adsorbed on Zr^{4+} ions in regular pores, where the coordination number had been reduced. Using *in-situ* XANES analysis, we monitored changes in the coordination sphere of zirconium in regular pores upon acetonitrile adsorption, finding that these changes were similar to those observed after water adsorption. This led us to conclude that acetonitrile occupies the vacant positions left by μ_3-OH groups. It is important to note that these Zr sites are present in any activated UiO-66, regardless of whether a linker or modulator is coordinated to the zirconium ions. Therefore, this hidden acidity is not associated with structural defects in UiO-66. In contrast, true acidity only occurs in locations where benzoates have been removed, reducing the number of ligands at the node compared to the ideal structure.

Next, we treated the samples with HCl and DMF to remove benzoate residues from the defective pores. DMF hydrolysis resulted in the formation of formic acid, which coordinated with Zr sites in the defect pores instead of benzoate residues. This substitution was traced using IR and Raman spectroscopy. Formate ions are much less bulky and can be partially decomposed during heating. In-situ FTIR analysis with CO and acetonitrile probe molecules showed that Zr ions in defective pores were now accessible and served as sites for the adsorption of probe molecules.

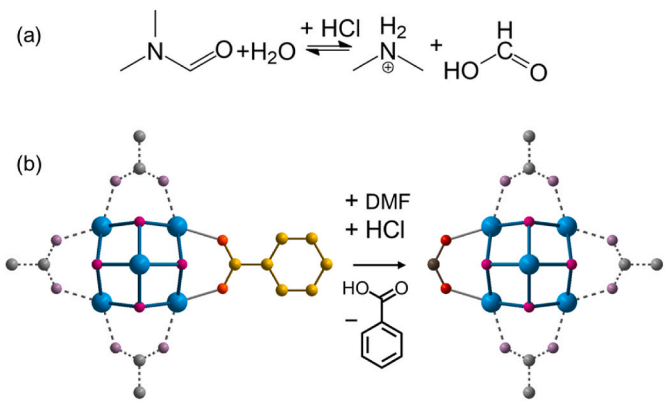

Fig. 11. (a) DMF hydrolysis in an acidic medium. (b) UiO-66 modification: HCl and DMF treatment with heating replaces benzoate residues in defect pores with formate. Gray spheres represent carbon, dusty-pink spheres represent oxygen, and dashed lines represent carboxylic bonds. Zirconium is coordinated with either benzoate or formate residues.

In conclusion, active sites in UiO-66 are highly desirable for imparting acidic properties to the framework. However, this MOF is a complex system whose active sites can vary depending on the synthesis and post-synthetic treatment. Site-specific methods such as *in-situ* IR analysis with probe molecules and XANES are essential for understanding these changes. Comprehensive analysis is crucial to accurately predicting and identifying active sites in UiO-66. Moreover, we precisely traced the process of UiO-66 modification, which allowed the introduction of Zr sites with increased Lewis acidity. These accessible sites can be used for attaching functional groups with specific properties to the MOF.

CRediT authorship contribution statement

Vera V. Butova: Writing – review & editing, Writing – original draft, Investigation, Formal analysis. **Videlina R. Zdravkova:** Investigation, Formal analysis. **Olga A. Burachevskaia:** Investigation, Formal analysis. **Ivan E. Gorban:** Investigation, Data curation. **Mikhail A. Soldatov:** Writing – review & editing, Validation, Methodology, Formal analysis. **Konstantin I. Hadjiivanov:** Writing – review & editing, Supervision, Funding acquisition, Data curation, Conceptualization.

Declaration of competing interest

The authors declare the following financial interests/personal relationships which may be considered as potential competing interests:

Vera Butova, Videlina Zdravkova, and Konstantin Hadjiivanov report that the Bulgarian Science Fund provided financial support. Mikhail Soldatov reports that the Southern Federal University provided financial support. Olga Burachevskaia reports that the Ministry of Science and Higher Education of the Russian Federation provided financial support.

Acknowledgments

We would like to express our gratitude to Dr. Prof. Svetlana Simova for her valuable contribution in performing the NMR measurements and for her insightful assistance in interpreting the obtained spectra.

The authors express their gratitude to the National Research Center

"Kurchatov Institute" for providing the beamtime at STM beamline and to Alexander Trigub for his valuable contributions to this research endeavor. The VVB, VRZ, and KIH would like to extend their appreciation to the Bulgarian Science Fund for their support of this work under grant number КП-06-ДВ-1. MAS acknowledges the Strategic Academic Leadership Program of the Southern Federal University ("Priority 2030") for synthesis support. OAB acknowledges the Ministry of Science and Higher Education of the Russian Federation for financial support (Agreement № 075-15-2021-1363) of spectral diagnostics.

Appendix A. Supplementary data

Supplementary data to this article can be found online at https://doi.org/10.1016/j.micromeso.2024.113372.

Data availability

Data will be made available on request.

References

[1] J.H. Cavka, S. Jakobsen, U. Olsbye, N. Guillou, C. Lamberti, S. Bordiga, K. P. Lillerud, A new zirconium inorganic building brick forming metal organic frameworks with exceptional stability, J. Am. Chem. Soc. 130 (2008) 13850–13851, https://doi.org/10.1021/ja8057953.

[2] S. Chavan, J.G. Vitillo, D. Gianolio, O. Zavorotynska, B. Civalleri, S. Jakobsen, M. H. Nilsen, L. Valenzano, C. Lamberti, K.P. Lillerud, et al., H_2 storage in isostructural UiO-67 and UiO-66 MOFs, Phys. Chem. Chem. Phys. 14 (2012) 1614–1626, https://doi.org/10.1039/C1CP23434J.

[3] F. Vermoortele, R. Ameloot, A. Vimont, C. Serre, D. De Vos, An amino-modified Zr-terephthalate metal–organic framework as an acid–base catalyst for cross-aldol condensation, Chem. Commun. 47 (2011) 1521–1523, https://doi.org/10.1039/C0CC03038D.

[4] A.L. Bugaev, A.A. Guda, K.A. Lomachenko, E.G. Kamyshova, M.A. Soldatov, G. Kaur, S. Oien-Odegaard, L. Braglia, A. Lazzarini, M. Manzoli, et al., Operando study of palladium nanoparticles inside UiO-67 MOF for catalytic hydrogenation of hydrocarbons, Faraday Discuss 208 (2018) 287–306, https://doi.org/10.1039/c7fd00224f.

[5] V.V. Butova, A.M. Aboraia, M. Solayman, I.S. Yahia, H.Y. Zahran, A.F. Abd El-Rehim, H. Algarni, G. Khabiri, A.V. Soldatov, The joint effect of naphthalene-system and defects on dye removal by UiO-66 derivatives, Microporous Mesoporous Mater. 325 (2021) 111314, https://doi.org/10.1016/j.micromeso.2021.111314.

[6] L. Valenzano, B. Civalleri, S. Chavan, S. Bordiga, M.H. Nilsen, S. Jakobsen, K. P. Lillerud, C. Lamberti, Disclosing the complex structure of UiO-66 metal organic framework: a synergic combination of experiment and theory, Chem. Mater. 23 (2011) 1700–1718, https://doi.org/10.1021/cm1022882.

[7] C. Atzori, G.C. Shearer, L. Maschio, B. Civalleri, F. Bonino, C. Lamberti, S. Svelle, K. P. Lillerud, S. Bordiga, Effect of benzoic acid as a modulator in the structure of UiO-66: an experimental and computational study, J. Phys. Chem. C 121 (2017) 9312–9324, https://doi.org/10.1021/acs.jpcc.7b00483.

[8] V.V. Butova, A.P. Budnyk, A.A. Guda, K.A. Lomachenko, A.L. Bugaev, A. V. Soldatov, S.M. Chavan, S. Øien-Ødegaard, U. Olsbye, K.P. Lillerud, et al., Modulator effect in UiO-66-NDC (1, 4-naphthalenedicarboxylic acid) synthesis and comparison with UiO-67-NDC isoreticular metal-organic frameworks, Cryst. Growth Des. 17 (2017) 5422–5431, https://doi.org/10.1021/acs.cgd.7b00892.

[9] V.V. Butova, K.S. Vetlitsyna-Novikova, I.A. Pankin, A.V. Soldatov, Formation of local defects and mesopores in a structure of UiO-66-NDC metal-organic framework, J. Surf. Invest. 14 (2020) 318–323, https://doi.org/10.1134/S1027451020020445.

[10] D.A. Giannakoudakis, T.J. Bandosz, Defectous UiO-66 MOF nanocomposites as reactive media of superior protection against toxic vapors, ACS Appl. Mater. Interfaces 12 (2020) 14678–14689, https://doi.org/10.1021/acsami.9b17314.

[11] S. Øien, D. Wragg, H. Reinsch, S. Svelle, S. Bordiga, C. Lamberti, K.P. Lillerud, Detailed structure analysis of atomic positions and defects in zirconium metal–organic frameworks, Cryst. Growth Des. 14 (2014) 5370–5372, https://doi.org/10.1021/cg501386j.

[12] R. Wei, C.A. Gaggioli, G. Li, T. Islamoglu, Z. Zhang, P. Yu, O.K. Farha, C.J. Cramer, L. Gagliardi, D. Yang, et al., Tuning the properties of Zr_6O_8 nodes in the metal organic framework UiO-66 by selection of node-bound ligands and linkers, Chem. Mater. 31 (2019) 1655–1663, https://doi.org/10.1021/acs.chemmater.8b05037.

[13] G.C. Shearer, S. Chavan, S. Bordiga, S. Svelle, U. Olsbye, K.P. Lillerud, Defect engineering: tuning the porosity and composition of the metal-organic framework UiO-66 via modulated synthesis, Chem. Mater. 28 (2016) 3749–3761, https://doi.org/10.1021/acs.chemmater.6b00602.

[14] D. Yang, M.A. Ortuño, V. Bernales, C.J. Cramer, L. Gagliardi, B.C. Gates, Structure and dynamics of Zr_6O_8 metal–organic framework node surfaces probed with ethanol dehydration as a catalytic test reaction, J. Am. Chem. Soc. 140 (2018) 3751–3759, https://doi.org/10.1021/jacs.7b13330.

[15] V.V. Butova, O.A. Burachevskaya, I.V. Ozhogin, G.S. Borodkin, A.G. Starikov, S. Bordiga, A. Damin, K.P. Lillerud, A.V. Soldatov, UiO-66 type MOFs with mixed-linkers - 1,4-Benzenedicarboxylate and 1,4-naphthalenedicarboxylate: effect of the modulator and post-synthetic exchange, Microporous Mesoporous Mater. 305 (2020) 110324, https://doi.org/10.1016/j.micromeso.2020.110324.

[16] A.A. Tereshchenko, V.V. Butova, A.A. Guda, O.A. Burachevskaya, A.L. Bugaev, A. N. Bulgakov, A.A. Skorynina, Y.V. Rusalev, I.V. Pankov, V.A. Volochaev, et al., Rational functionalization of UiO-66 with Pd nanoparticles: synthesis and in situ fourier-transform infrared monitoring, Inorg. Chem. 61 (2022) 3875–3885, https://doi.org/10.1021/acs.inorgchem.1c03340.

[17] V.V. Butova, V.R. Zdravkova, O.A. Burachevskaia, A.A. Tereshchenko, P. S. Shestakova, K.I. Hadjiivanov, In situ FTIR spectroscopy for scanning accessible active sites in defect-engineered UiO-66, Nanomaterials 13 (2023) 1675, https://doi.org/10.3390/nano13101675.

[18] G.C. Shearer, J.G. Vitillo, S. Bordiga, S. Svelle, U. Olsbye, K.P. Lillerud, Functionalizing the defects: postsynthetic ligand exchange in the metal organic framework UiO-66, Chem. Mater. 28 (2016) 7190–7193, https://doi.org/10.1021/acs.chemmater.6b02749.

[19] K. Chakarova, I. Strauss, M. Mihaylov, N. Drenchev, K. Hadjiivanov, Evolution of acid and basic sites in UiO-66 and UiO-66-NH_2 metal-organic frameworks: FTIR study by probe molecules, Microporous Mesoporous Mater. 281 (2019) 110–122, https://doi.org/10.1016/j.micromeso.2019.03.006.

[20] V. Petříček, M. Dušek, L. Palatinus, Crystallographic computing system JANA2006: general features, Z. Kristallogr. 229 (2014) 345–352, https://doi.org/10.1515/zkri-2014-1737.

[21] A.A. Chernyshov, A.A. Veligzhanin, Y.V. Zubavichus, Structural materials science end-station at the Kurchatov Synchrotron radiation Source: recent instrumentation upgrades and experimental results, Nucl. Instrum. Methods Phys. Res., Sect. A 603 (2009) 95–98, https://doi.org/10.1016/j.nima.2008.12.167.

[22] B. Ravel, M. Newville, ATHENA, ARTEMIS, HEPHAESTUS: Data analysis for X-ray absorption spectroscopy using IFEFFIT, in: Proceedings of the Journal of Synchrotron Radiation, 2005, pp. 537–541.

[23] M.H. Borawska, P. Koczoń, J. Piekut, R. Świsłocka, W. Lewandowski, Vibrational spectra and antimicrobial activity of selected bivalent cation benzoates, J. Mol. Struct. 919 (2009) 284–289, https://doi.org/10.1016/j.molstruc.2008.09.018.

[24] D. Stoilova, V. Koleva, IR study of solid phases formed in the $Mg(HCOO)_2$–$Cu(HCOO)_2$–H_2O system, J. Mol. Struct. 553 (2000) 131–139, https://doi.org/10.1016/S0022-2860(00)00541-X.

[25] V.Z. Vassileva, P.P. Petrova, Formation and characterization of bisthiourea zinc formate, in: Proceedings of the Croatica Chemical Acta, 2005, pp. 295–299.

[26] K.I. Hadjiivanov, D.A. Panayotov, M.Y. Mihaylov, E.Z. Ivanova, K.K. Chakarova, S. M. Andonova, N.L. Drenchev, Power of infrared and Raman spectroscopies to characterize metal-organic frameworks and investigate their interaction with guest molecules, Chem. Rev. 121 (2021) 1286–1424, https://doi.org/10.1021/acs.chemrev.0c00487.

[27] J.R.S. Brownson, M.I. Tejedor-Tejedor, M.A. Anderson, FTIR spectroscopy of alcohol and formate interactions with mesoporous TiO_2 surfaces, J. Phys. Chem. B 110 (2006) 12494–12499, https://doi.org/10.1021/jp0614547.

[28] Z. Lu, J. Liu, X. Zhang, Y. Liao, R. Wang, K. Zhang, J. Lyu, O.K. Farha, J.T. Hupp, Node-accessible zirconium MOFs, J. Am. Chem. Soc. 142 (2020) 21110–21121, https://doi.org/10.1021/jacs.0c09782.

[29] J.E. Mondloch, W. Bury, D. Fairen-Jimenez, S. Kwon, E.J. DeMarco, M.H. Weston, A.A. Sarjeant, S.T. Nguyen, P.C. Stair, R.Q. Snurr, et al., Vapor-phase metalation by atomic layer deposition in a metal–organic framework, J. Am. Chem. Soc. 135 (2013) 10294–10297, https://doi.org/10.1021/ja4050828.

[30] M. Athar, P. Rzepka, D. Thoeny, M. Ranocchiari, J. Anton van Bokhoven, Thermal degradation of defective high-surface-area UiO-66 in different gaseous environments, RSC Adv. 11 (2021) 38849–38855, https://doi.org/10.1039/D1RA05411B.

[31] C. Volkringer, H. Leclerc, J.-C. Lavalley, T. Loiseau, G. Férey, M. Daturi, A. Vimont, Infrared spectroscopy investigation of the acid sites in the metal–organic framework aluminum trimesate MIL-100(Al), J. Phys. Chem. C 116 (2012) 5710–5719, https://doi.org/10.1021/jp210671t.

[32] D.M. Driscoll, D. Troya, P.M. Usov, A.J. Maynes, A.J. Morris, J.R. Morris, Characterization of undercoordinated Zr defect sites in UiO-66 with vibrational spectroscopy of adsorbed CO, J. Phys. Chem. C 122 (2018) 14582–14589, https://doi.org/10.1021/acs.jpcc.8b03283.

[33] V.V. Torbina, M.A. Salaev, E.A. Paukshtis, L.F. Liotta, O.V. Vodyankina, Effect of linker substituent nature on performance of active sites in UiO-66: combined FT-IR and DFT study, Int. J. Mol. Sci. 24 (2023), https://doi.org/10.3390/ijms241914893.

[34] D.M. Driscoll, D. Troya, P.M. Usov, A.J. Maynes, A.J. Morris, J.R. Morris, Geometry and energetics of CO adsorption on hydroxylated UiO-66, Phys. Chem. Chem. Phys. 21 (2019) 5078–5085, https://doi.org/10.1039/C8CP07778A.

[35] E.P.L. Hunter, S.G. Lias, Evaluated gas phase basicities and proton affinities of molecules: an update, J. Phys. Chem. Ref. Data 27 (1998) 413–656, https://doi.org/10.1063/1.556018.

[36] M. Cascella, S. Raugei, P. Carloni, Formamide hydrolysis investigated by multiple-steering ab initio molecular dynamics, J. Phys. Chem. B 108 (2004) 369–375, https://doi.org/10.1021/jp035458c.